

# Systems biology approaches identify ATF3 as a negative regulator of Toll-like receptor 4

Mark Gilchrist<sup>1</sup>, Vesteynn Thorsson<sup>1</sup>, Bin Li<sup>1</sup>, Alistair G. Rust<sup>1</sup>, Martin Korb<sup>1</sup>, Kathleen Kennedy<sup>1</sup>, Tsonwin Hai<sup>2</sup>, Hamid Bolouri<sup>1</sup> & Alan Aderem<sup>1</sup>

The innate immune system is absolutely required for host defence, but, uncontrolled, it leads to inflammatory disease. This control is mediated, in part, by cytokines that are secreted by macrophages. Immune regulation is extraordinarily complex, and can be best investigated with systems approaches (that is, using computational tools to predict regulatory networks arising from global, high-throughput data sets). Here we use cluster analysis of a comprehensive set of transcriptomic data derived from Toll-like receptor (TLR)-activated macrophages to identify a prominent group of genes that appear to be regulated by activating transcription factor 3 (ATF3), a member of the CREB/ATF family of transcription factors. Network analysis predicted that ATF3 is part of a transcriptional complex that also contains members of the nuclear factor (NF)- $\kappa$ B family of transcription factors. Promoter analysis of the putative ATF3-regulated gene cluster demonstrated an over-representation of closely apposed ATF3 and NF- $\kappa$ B binding sites, which was verified by chromatin immunoprecipitation and hybridization to a DNA microarray. This cluster included important cytokines such as interleukin (IL)-6 and IL-12b. ATF3 and Rel (a component of NF- $\kappa$ B) were shown to bind to the regulatory regions of these genes upon macrophage activation. A kinetic model of *Il6* and *Il12b* messenger RNA expression as a function of ATF3 and NF- $\kappa$ B promoter binding predicted that ATF3 is a negative regulator of *Il6* and *Il12b* transcription, and this hypothesis was validated using *Atf3*-null mice. ATF3 seems to inhibit *Il6* and *Il12b* transcription by altering chromatin structure, thereby restricting access to transcription factors. Because ATF3 is itself induced by lipopolysaccharide, it seems to regulate TLR-stimulated inflammatory responses as part of a negative-feedback loop.

The innate immune system is the body's first line of defence against infection. It identifies foreign invaders using pattern recognition receptors, which detect highly conserved microbial-specific structures (PAMPs)<sup>1–4</sup>; the TLRs are prototypic pattern recognition receptors<sup>5</sup>. Macrophages, activated via TLRs, unfold a tightly controlled pathogen-specific immune response<sup>6</sup>. Much is known about the activation of macrophages leading to the transcription of single genes. For example, it is well known that the transcription factor NF- $\kappa$ B has a central role in TLR4-induced transcription of cytokines such as IL-6 and IL-12b. However, TLR activation involves a complex transcriptional programme with changes in >1,000 genes, and our overall understanding of both positive and negative transcriptional control is woefully inadequate<sup>7</sup>. The tools of systems biology are well suited to investigate the complex interactions induced in macrophages by TLR activation; global transcription can be measured using complementary DNA microarrays, and computational analysis of this information can lead to a deeper understanding of the system as a whole<sup>2,3</sup>. We report here on a novel self-regulatory mechanism in the TLR pathway identified by global analysis of successive waves of transcriptional activity induced during macrophage activation.

## Transcriptional profiling of LPS-stimulated macrophages

Temporal activation of macrophages by the TLR4 agonist bacterial lipopolysaccharide (LPS) was analysed using cDNA microarrays. These data were clustered to reveal prominent groups of genes with

similar changes in expression pattern using a *k*-means algorithm (Fig. 1). Eleven clusters comprising regulated 'waves' of transcription with early, intermediate and late phases were defined. We were particularly interested in identifying early clusters of transcription factors, because these were likely to control subsequent rounds of transcriptional activation. Cluster 6 met these criteria; it contained several transcription factors (ATF3, Btg2, Egr1, Egr2, Fos, Ier2, Jun and Rel) whose mRNA expression peaked at 1 h (Fig. 1 and Supplementary Data 1). We hypothesized that these clustered genes are co-regulated<sup>8</sup> and that they share *cis*-regulatory elements. *Cis*-regulatory analysis using MotifMogul (<http://labs.systemsbio.net/bolouri/Mogul/>; see below) predicted over-representation of ATF/CREB binding sites in cluster 6. Although it is not yet possible to differentiate computationally between the DNA binding sites of the ATF/CREB transcription factors, ATF3 was the likely candidate as it was the only member of the family that was induced after LPS stimulation of macrophages (Supplementary Data 2, Fig. 2S1). ATF3 has not previously been implicated in regulation of the immune response. It is a member of the CREB family of basic leucine zipper transcription factors, and has been shown to act both as a transcriptional activator or repressor depending on the cell type and stimulus<sup>9</sup>. The biological role of ATF3 is also obscure. It has been reported to function in the stress response, the regulation of the cell cycle, and in apoptosis<sup>9–14</sup>, although the details of how this occurs are scant and contradictory. For example, ATF3 has been implicated both as a tumour suppressor<sup>10</sup> and as an

<sup>1</sup>Institute for Systems Biology, Seattle, Washington 98103, USA. <sup>2</sup>Department of Molecular and Cellular Biochemistry, Ohio State University, Columbus, Ohio 43210, USA.

augmenter of metastasis in a murine melanoma model<sup>11</sup>. It has also been implicated to be either pro- or anti-apoptotic. For example, on the one hand, mouse embryonic fibroblasts derived from *Atf3*<sup>-/-</sup> mice are partially protected from stress-induced apoptosis<sup>12</sup>. On the other hand, ATF3 protects endothelial cells from tumour-necrosis factor (TNF)-induced apoptosis by decreasing the transcription of p53 (ref. 13).

### ATF3 regulatory complex and transcriptional targets

In order to determine the role of ATF3 in TLR signalling we first needed to identify the components of the putative ATF3 regulatory complex. Our strategy was to use computational tools to predict members of the complex, and then to validate the prediction using biological methods. Potential ATF3-interacting proteins were identified using a protein–protein interaction map displayed in Cytoscape (<http://www.cytoscape.org/>), a network analysis and visualization tool<sup>4,15</sup> (Fig. 2a; the nodes (circles) represent proteins and the edges (lines) represent direct interactions between the proteins). The protein–protein interactions visualized in Cytoscape are largely curated from the literature, and, as such, they represent possible interactions. Notably, ATF3 is predicted to interact with two major transcriptional complexes known to be involved in TLR signalling: NF- $\kappa$ B (p50) and AP1 (Jun, Junb, Jun1 and Fos) (Fig. 2a). We chose Rel as a surrogate for NF- $\kappa$ B as it co-segregated with ATF3 in cluster 6. Jun and Fos are also members of cluster 6 and they were therefore chosen to represent AP1. Again we used MotifMogul, this time to identify enriched ATF3, NF- $\kappa$ B and AP1 binding site densities and their proximity to each other and to the transcriptional start sites of potential target genes in cluster 2 (that is, the cluster of genes that was activated immediately after the induction of the transcription factors in cluster 6). Using these constraints we identified 30 target genes that contained putative ATF3 sites within 100 base pairs (bp) of NF- $\kappa$ B binding sites and located within 500 bp of the transcriptional start site (Supplementary Data 3 and 4). Of this subset, IL-6 and IL-12b were chosen for further investigation because of their biological relevance (Fig. 2b).

### ATF3 kinetic model in LPS-induced gene transcription

We then validated the predicted ATF3 and Rel binding sites on the regulatory regions of the genes encoding IL-6 and IL-12b using chromatin immunoprecipitation (ChIP) (Fig. 3a). Rel bound to the *Il6* and *Il12b* promoters within 1 h of LPS stimulation, and this binding declined after 2 h. ATF3 binding occurred more slowly, with maximal binding at 4 h. In contrast to Rel, ATF3 binding did not decline, and remained constant at 6 h (Fig. 3a). The binding of ATF3 and Rel to their cognate promoters mirrored the nuclear concentration of these transcription factors (Fig. 3b).

To characterize further the function of ATF3 in the TLR pathway we searched for functionally predictive kinetic relationships between the binding of Rel and ATF3 to the *Il6* promoter and *Il6* expression. Using a generalized multivariate regression model<sup>16,17</sup>, *Il6* transcription levels are determined by the amount of promoter-bound ATF3 and Rel; these combine additively with weight coefficients  $\beta_{\text{Rel}}$  and  $\beta_{\text{ATF3}}$ , the numerical values of which can be estimated by fitting the model to the data (see Methods). These parameters describe the relative influence of each transcription factor in determining *Il6* expression, and are estimated from the *Il6* expression and transcription factor occupancy on the *Il6* promoter. A positive coefficient implies that the transcription factor has the role of an activator, whereas a negative coefficient implies repression. Fitting the parameters yields  $\beta_{\text{Rel}} = 7.8$  and  $\beta_{\text{ATF3}} = -4.9$ , suggesting that Rel and ATF3 are both important in determining *Il6* expression levels, and that Rel is a transcriptional activator (consistent with current knowledge) whereas ATF3 is a negative regulator of *Il6* expression (Supplementary Data 5a). To explore further this prediction we simulated *Atf3*-null conditions by removing the corresponding term in the kinetic equation (Fig. 3c). The model predicts that *Il6* expression is substantially increased in *Atf3*-null conditions, and, in contrast to the wild type, the transcription of *Il6* is not inhibited, but continues to rise (Fig. 3c). An exhaustive search of the biologically plausible range of values for these parameters revealed only one possible answer: that ATF3 is a negative regulator of LPS-induced *Il6* expression (Fig. 3d). Similar conclusions were derived from analysis of the *Il12b* gene with

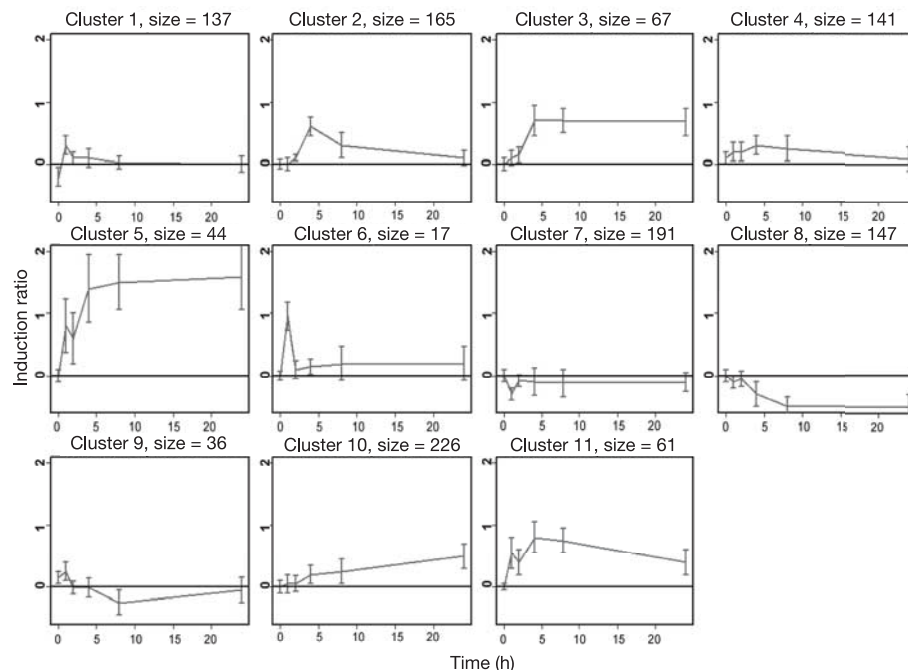


**Figure 1 | Macrophage genes regulated by LPS form distinct kinetic clusters.** Macrophages were stimulated with  $10 \text{ ng ml}^{-1}$  LPS and RNA was isolated at the indicated times and subjected to microarray analysis. Genes were clustered by their kinetic profiles using a *k*-means algorithm using

average  $\log_{10}$  values of normalized gene expression ratios. Data represent the average of three independent experimental values  $\pm$  standard error. The transcription factor constituents of cluster 6, which show an early peak of mRNA expression, are ATF3, Btg2, c-Jun, c-Fos, Egr1, Egr2, Ier2 and c-Rel.

fitting parameters of  $\beta_{Rel} = 18.5$  and  $\beta_{Atf3} = -9.6$  (Supplementary Data 5, Figs S51 and S52).

**Biological effects of ATF3**

To clarify the function of ATF3 in TLR4 signalling and to test our predictions, we obtained *Atf3*<sup>-/-</sup> mice for further study<sup>14</sup>. These mice develop normally and show no overt immunological phenotype in specific pathogen-free conditions. Quantitative real-time polymerase chain reaction with reverse transcription (RT-PCR) revealed a substantial increase in LPS-induced *Il6* and *Il12b* mRNA levels in *Atf3*<sup>-/-</sup> bone-marrow derived macrophages (BMMs) (Fig. 4a). LPS induction of *iNOS* and *Tnf* mRNA was similarly enhanced in *Atf3*<sup>-/-</sup> mice. However, mRNA levels encoding MIP2 were unaffected in *Atf3*<sup>-/-</sup> mice, demonstrating selectivity of the ATF3 effect (Fig. 4a). The increases in mRNA were mirrored by cytokine secretion and NO production (Fig. 4b). Similar effects were noted in resident peritoneal macrophages as well as in liver (Supplementary Data 2, Figs 2S2 and 2S3). The inhibitory role of ATF3 in LPS-induced responses in BMMs in culture was even more pronounced *in vivo*. Circulating levels of IL-6

and IL-12b were increased more than 10-fold in *Atf3*<sup>-/-</sup> mice receiving LPS intraperitoneally (Fig. 4c) compared with wild-type counterparts. Serum TNF levels were similarly increased (Supplementary Data 2, Fig. 2S4). Survival in this *in vivo* endotoxemic shock model was also substantially altered: whereas 100% of *Atf3*<sup>-/-</sup>

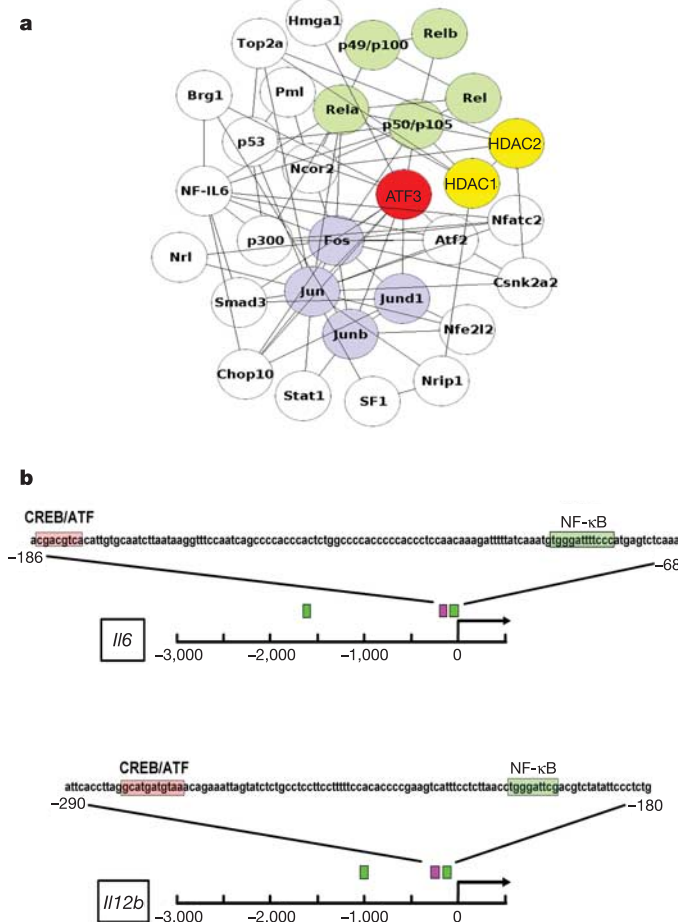


**Figure 2 | Predicting ATF3 target genes using protein interaction network and promoter analysis.** **a**, ATF3-associated transcription factors are determined from the known transcription factor protein-protein interaction network using Cytoscape. ATF3 (red) is predicted to interact with a number of transcription factors, including members of the AP1 (light blue) and NF-κB (light green) transcription factor complexes. **b**, Computational analysis of the regulatory elements of *Il6* and *Il12b*. ATF3/CREB and NF-κB binding sites were identified by scanning the 5' promoter regions of the *Il6* and *Il12b* genes with MotifMogul. Each coloured block represents a match: red blocks are ATF/CREB sites; green blocks are NF-κB sites. The numbers on the axis refer to bases 5' upstream from transcription start site.

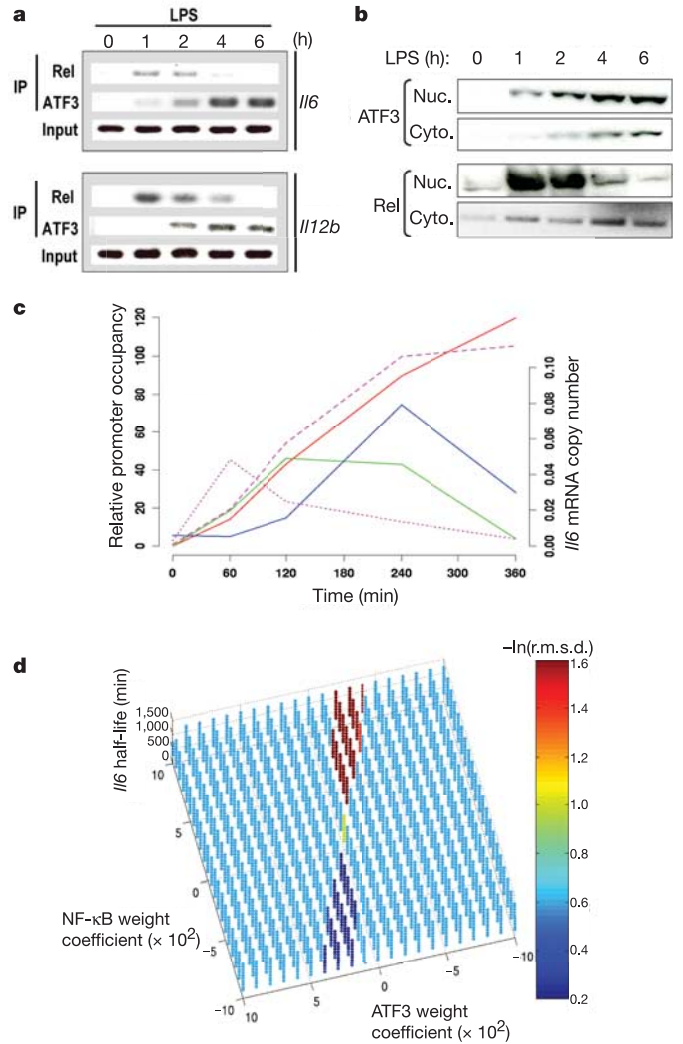


**Figure 3 | Kinetic analysis predicts a negative regulatory role for ATF3 in LPS-stimulated responses.** **a**, Temporal recruitment of ATF3 and Rel to the *Il6* and *Il12b* promoters. Macrophages from wild-type mice were stimulated with 10 ng ml<sup>-1</sup> LPS for the indicated times. ChIP assays were performed. DNA from input or immunoprecipitated (IP) fractions was measured by PCR amplification of specific promoter sequences. **b**, Protein expression and localization of ATF3 and Rel. Macrophages from wild-type mice were stimulated with 10 ng ml<sup>-1</sup> LPS for the indicated times. Nuclear and cytosolic extracts were analysed by immunoblotting. **c**, Kinetics of *Il6* regulation by Rel and ATF3. Kinetic transcription factor binding data for Rel and ATF3 in LPS-stimulated macrophages was determined from chromatin immunoprecipitation (Rel (dotted purple line) and ATF3 (dashed purple line)), and plotted together with *Il6* mRNA levels as determined by real-time PCR (blue solid line). Two parameters were optimized,  $\beta_{Rel} = 7.8$  and  $\beta_{Atf3} = -4.9$ , representing the relative contributions of Rel and ATF3 levels in determining *Il6* transcription. Shown by the green solid line are the predicted *Il6* levels derived from the kinetic model. Omitting the ATF3 term in the model gives a prediction of *Il6* levels in an *Atf3* knockout (red solid line). **d**, Visualization of the parameter space of the kinetic model of *Il6* regulation. The space of biologically plausible parameter values was visualized as a three dimensional grid. The fit is best in the red region to the top and right of the plot, and worst in the dark blue region (to the bottom left of the figure).

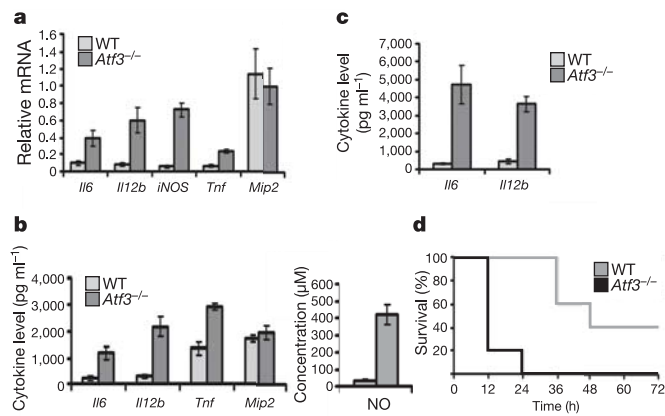


**Figure 4 | Role of ATF3 in *in vitro* and *in vivo* LPS responses.** **a**, BMMs were stimulated with  $10 \text{ ng ml}^{-1}$  LPS for 4 h and the indicated cytokines were measured by quantitative real-time RT-PCR analysis. Data represent the average of three independent experimental values  $\pm$  standard error. WT, wild-type mice (C57BL/6). **b**, BMMs were stimulated with  $10 \text{ ng ml}^{-1}$  LPS for 4 h and cytokine levels determined by ELISA (left) and nitric oxide determined by Griess assay (right). Data represent the average of three independent experimental values  $\pm$  standard error. **c**, Wild-type or *Atf3*<sup>-/-</sup> mice were injected intraperitoneally with LPS ( $20 \text{ mg kg}^{-1}$ ), serum was drawn at 12 h and analysed by ELISA. Data represent the average of three values  $\pm$  standard error. **d**, Age-matched wild-type and *Atf3*<sup>-/-</sup> mice ( $n = 10$ ) were injected intraperitoneally with LPS ( $20 \text{ mg kg}^{-1}$ ) and then monitored for survival.

mice had succumbed by 24 h after LPS administration, none of the wild-type mice had expired at this early time point (Fig. 4d).

### Functional mechanism of ATF3

We next explored the mechanism by which ATF3 inhibits LPS-induced transcription. Chromatin remodelling regulates transcription by allowing, or preventing, access of transcription factors to their cognate binding sites. The protein-protein interaction map demonstrates connectivity of ATF3 with histone deacetylase (HDAC; yellow nodes) via the NF- $\kappa$ B complex (Fig. 2a). HDAC has a critical role in chromatin remodelling by participating in the acetylation/deacetylation cycle of histones: acetylation relaxes chromatin structure thereby allowing access of transcription factors to DNA, conversely, deacetylation alters chromatin structure to limit transcription factor access. LPS treatment of macrophages resulted in a substantial increase in HDAC activity that could be co-precipitated with ATF3 (Fig. 5a, left panel), and western blotting demonstrated the presence of HDAC1 in the immunoprecipitated complex (Fig. 5a, right panel). We assessed the effect of ATF3-dependent chromatin remodelling on the *Il6* and *Il12b* promoters by determining histone acetylation status using ChIP. Acetylated histone H4 (H4ac), an indicator of open chromatin structure, bound to the *Il6* promoter within 1 h of LPS treatment (Fig. 5b). The kinetics of the association of H4ac with the *Il6* promoter mirrored the binding of Rel to this promoter (compare Figs 5b and 3a), strongly suggesting that the open chromatin structure permits access of Rel to its DNA binding site. After 2 h the amount of promoter-bound H4ac decreased, with a temporal response similar to the decrease in Rel binding (Figs 5b and 3a). These kinetics mirror the association of ATF3 with the *Il6* promoter, and the observation that deacetylation of histone H4 does not occur in *Atf3*<sup>-/-</sup> macrophages strongly suggests that ATF3-associated HDAC1 is responsible for this deacetylation (Figs 5a, b and 3a). Similar results were obtained for the association of H4ac with the *Il12b* promoter, and for acetylated histone H3 on both promoters (data not shown). The observation that the HDAC inhibitor trichostatin A increased LPS-induced transcription of *Il6* and *Il12b* in a similar manner to that seen in *Atf3*<sup>-/-</sup> macrophages further suggested that ATF3 inhibits transcription via chromatin remodelling (Fig. 5c).

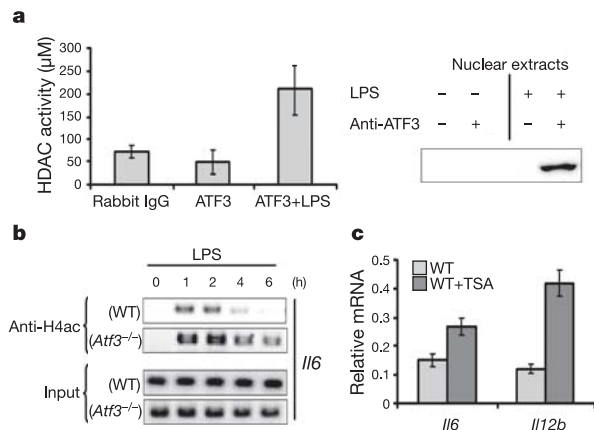


**Figure 5 | Role of HDAC in ATF3-mediated gene regulation.** **a**, Left panel: BMMs from wild-type mice were stimulated with  $10 \text{ ng ml}^{-1}$  LPS for 6 h and immunoprecipitation with relevant antibody and associated HDAC activity measured by colorimetric assay. Data represent the average of three independent experimental values  $\pm$  standard error. Right panel: complex formation of ATF3 and HDAC1 *in vivo*. BMMs from wild-type mice were stimulated with  $10 \text{ ng ml}^{-1}$  LPS for 6 h and nuclear extracts were isolated and immunoprecipitated with anti-ATF3 antibody and immunoblotted with anti-HDAC1. **b**, Dynamics of H4 acetylation on the *Il6* promoter. Macrophages from wild-type or *Atf3*<sup>-/-</sup> mice were stimulated with  $10 \text{ ng ml}^{-1}$  LPS for the indicated times. ChIP assays were performed using anti-acetyl H4 antibody as described in the Methods. **c**, Treatment with HDAC inhibitor potentiates macrophage cytokine gene transcription. BMMs from wild-type mice (C57BL/6) were treated with the HDAC inhibitor trichostatin A (TSA,  $100 \text{ ng ml}^{-1}$ ) and  $10 \text{ ng ml}^{-1}$  LPS for 4 h and the cytokines measured by quantitative real-time RT-PCR analysis. Data represent the average of three independent experimental values  $\pm$  standard error.

Taken together, the data suggest that LPS-induced acetylation of histones opens chromatin structure to allow access of Rel to the *Il6* and *Il12b* promoters and activation of transcription. ATF3 subsequently binds to these promoters, and ATF3-associated HDAC1 deacetylates histones, resulting in the closure of chromatin and the inhibition of transcription. This mechanism is indirectly supported by a recent publication demonstrating that ATF3 $\Delta$ Zip2, a splice variant of ATF3 lacking DNA-binding activity, sensitizes cells to apoptosis by sequestering CREB-binding protein-p300 (ref. 18). Because CREB-binding protein-p300 form a scaffold for histone acetyltransferase (HAT)<sup>19</sup>, their sequestration would indirectly result in a lack of histone acetylation. Thus, it is possible that ATF3 may modify transcription by two independent mechanisms involving histone acetylation: first, in a DNA-dependent manner by directly recruiting a histone deacetylase to promoters containing an ATF3 binding site, and second, in a DNA-independent manner by ATF3 $\Delta$ Zip2, which sequesters the HAT complex, thus indirectly preventing histone acetylation.

### ATF3 transcriptional network

Our data demonstrate that ATF3 and Rel jointly regulate LPS-induced *Il6*, *Il12b* and *iNOS* transcription. We used ChIP-to-chip analysis (see below) to examine whether ATF3 binds to the *cis*-regulatory elements of the remaining 27 genes (listed in Supplementary Data 3, Table S3.1) that were computationally predicted to be its targets. DNA segments bound by ATF3 were chromatin immunoprecipitated (ChIP) and hybridized to a DNA microarray (chip) containing 25-mer oligonucleotide probes tiling the proximal promoters of selected genes at a density of approximately every 20–30 bases. Eleven genes with significantly increased ATF3 binding were identified (Supplementary Data 8, Fig. S8a–c). We cross-validated this set against a set of 15 genes that are upregulated in *Atf3*<sup>-/-</sup> macrophages, obtained using Affymetrix microarrays. As shown in Fig. 6a, 11 genes are significantly

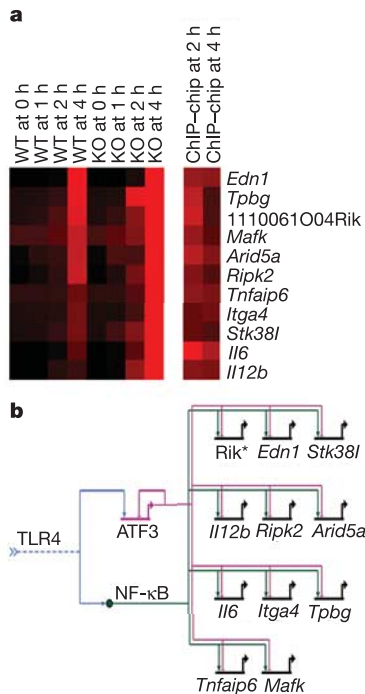


**Figure 6 | The transcriptional regulatory network of ATF3.** **a**, Correlation of the ATF3 DNA binding profiles with gene expression patterns. Macrophages from wild-type or *Atf3*<sup>-/-</sup> mice were stimulated with 10 ng ml<sup>-1</sup> LPS and RNA was isolated at the indicated times and subjected to microarray analysis. ChIP binding data (at 2 h and 4 h) were derived from wild-type macrophages stimulated with 10 ng ml<sup>-1</sup> LPS. Heat map colour for expression arrays is based on normalized fold changes among eight conditions on each gene (from no expression (black) through to high expression (bright red)). ChIP-to-chip results are based on normalized peak ratios of identified segments for the 11 genes. **b**, Proposed ATF3 regulatory network in LPS-stimulated macrophages visualized using Biotaepstry software (<http://www.biotaepstry.org>). ATF3 and NF-κB are both activated by TLR4 signalling and jointly regulate the transcription of a battery of downstream genes. Rik\*, 1110061O04Rik.

upregulated in *Atf3*<sup>-/-</sup> macrophages and directly bound by ATF3. Taken together, these data suggest that ATF3 is a transcriptional repressor of the genes in Fig. 6a. Figure 6b is a network diagram incorporating the findings reported in this paper. Thus, ATF3 and NF-κB are both induced by TLR4 signalling and jointly regulate a battery of downstream genes. Because ATF3 is itself induced by LPS, it seems to regulate TLR-stimulated inflammatory responses as part of a negative feedback loop.

## METHODS

**Mouse bone-marrow-derived macrophages.** *Atf3*<sup>-/-</sup> mice in the C57BL/6 background were generated by backcrossing *Atf3*<sup>-/-</sup> mice in the 129SVJ background to C57BL/6 mice, ten times<sup>14</sup>. Bone marrow was collected from femurs in complete RPMI containing 10% heat-inactivated FCS (Hyclone Laboratories), 100 U ml<sup>-1</sup> penicillin, 100 μg ml<sup>-1</sup> streptomycin, 2 mM L-glutamine and 50 ng ml<sup>-1</sup> rmM-CSF (R&D Systems). BMMs were stimulated with high purity LPS (10 ng ml<sup>-1</sup>) for the indicated times. As a model of LPS-induced septic shock, mice were injected intraperitoneally with 20 mg kg<sup>-1</sup> LPS. The University of Washington and Institute for Systems Biology's Institutional Animal Care and Use Committees approved all animal protocols.

**Affymetrix GeneChip analysis and quantitative real-time PCR.** Total RNA was isolated using Trizol (Invitrogen) and analysed by real-time PCR with probes (IDT) labelled with 5' FAM and 3' TAMRA. Data were normalized by the level of EF1a expression in individual samples. Primer sequences are available upon request. The Affymetrix protocol was essentially as described. cRNA was hybridized for 16 h to Affymetrix MG-U74Av2 arrays (Affymetrix), which contain ~45,101 mouse probe sets, half of which correspond to expressed sequence tags (ESTs) and half to characterized genes. Normalization was performed using GeneChip robust multi-array analysis, followed by GC-robust

multi-array average (GC-RMA) normalization. Identification of significantly perturbed genes was done using significance analysis of microarrays. The false positive rate was 0.1%.

**Immunoblotting.** Whole-cell and nuclear/cytosolic extracts of BMMs were prepared as previously described<sup>20</sup>. Antibodies against the following proteins were purchased as indicated: ATF3 (Santa Cruz), Rel (Santa Cruz), acetylated histone H3 (Upstate) and acetylated histone H4 (Upstate).

**Chromatin immunoprecipitation assay.** After stimulation, BMMs were fixed in formaldehyde and ChIP was performed. The antibodies used for immunoprecipitation were as listed above. The purified DNA was analysed by PCR using primers specific for the *Il6* and *Il12b* promoters. The PCR products were visualized on an ethidium bromide gel. The levels of promoter-bound ATF3 and Rel were determined by band densitometry for use in kinetic modelling. A detailed protocol is noted in Supplementary Data 6.

**ELISA.** Cytokine release were determined with a sandwich enzyme-linked immunosorbent assay (ELISA) technique (Duoset; R&D Systems) using the manufacturer's recommended protocol.

**MotifMogul.** We scanned the promoter regions of genes from -3,000 bp to +500 bp of the transcriptional starting site (NCBI m33 mouse assembly). Three scanning methods—MotifLocator<sup>21</sup>, MotifScanner<sup>21</sup> and Clover<sup>22</sup>—were applied using known TRANSFAC motifs to search ATF/CREB, NF-κB and AP1 binding sites (Professional version 8.3)<sup>23</sup>. Because ATF binding sites have strong overlap with CREB binding sites, we scanned using a combined matrix set including three ATF matrices and nine CREB matrices. MotifMogul is used to integrate the three scanning methods, and default parameters of each individual algorithm were applied. Only statistically significant sites, as determined against a randomly derived DNA sequence, are filtered and examined. Matrix matches were visualized using the Apollo genome annotation viewer<sup>24</sup>.

**Cytoscape.** Cytoscape, our network visualization program, overlays cDNA expression profiles on a matrix of protein–protein and protein–DNA interaction networks. Our Cytoscape database contains 5,200 known protein–protein and protein–DNA interactions, and 17,600 relationships between these proteins (mostly curated from the literature). For a comprehensive description of these programs, see <http://www.systemsbio.org>.

**Kinetic model.** We used a generalized multivariate regression model<sup>16,17</sup> to model the kinetics of transcriptional regulation of *Il6* or *Il12b* by ATF3 and Rel:

$$\tau \frac{d(Il6)}{dt} = -Il6 + g(\beta_{Rel}Rel + \beta_{ATF3}ATF3) \quad (1)$$

In equation (1), the term *Il6* represents the level of *Il6* mRNA expression as determined by real-time PCR, whereas the terms *Rel* and *ATF3* represent the levels of Rel and ATF3 bound to the *Il6* promoter, as determined by ChIP. The weight parameters  $\beta_{Rel}$  and  $\beta_{ATF3}$ , estimated from the data, are the relative contributions of Rel and ATF3 in determining *Il6* transcription according to the model. The function *g* is a sigmoidal transfer function<sup>17</sup>, incorporating lower and upper bounds on *Il6* expression. The parameter  $\tau$  was fixed for consistency with  $T^{1/2} = 600$  min, a representative mRNA half-life in mammalian cells<sup>25</sup>. The kinetic equation was discretized at the measured time intervals<sup>17</sup>, and the optimal parameters were found to be  $\beta_{Rel} = 7.8$  and  $\beta_{ATF3} = -4.9$ , by least squares regression. We verified that the signs of the two terms were preserved for a range of mRNA half-lives. Results for *Il12b* were obtained by a similar process.

**Assay for HDAC activity.** HDAC activity was measured by a non-isotopic assay (Biomol) using a chromagen linked acetylated substrate according to the manufacturer's protocol.

**ChIP-to-chip analysis.** We designed a custom oligonucleotide array containing densely tiled 25-mer oligonucleotide sequences designed to interrogate genes that were identified to be of probable importance for immune activation. For ChIP-to-chip binding analysis, we used an approach similar to previous publications<sup>26,27</sup>, including quantile normalization<sup>26</sup> and median-based filtering with identification of ATF3 binding sites<sup>27</sup>.

Received 28 February; accepted 29 March 2006.

1. Kawai, T. & Akira, S. Pathogen recognition with Toll-like receptors. *Curr. Opin. Immunol.* **17**, 338–344 (2005).
2. Aderem, A. Systems biology: its practice and challenges. *Cell* **121**, 511–513 (2005).
3. Kitano, H. Computational systems biology. *Nature* **420**, 206–210 (2002).
4. Suthram, S., Sittler, T. & Ideker, T. The plasmodium protein network diverges from those of other eukaryotes. *Nature* **438**, 108–112 (2005).
5. Royet, J., Reichhart, J. M. & Hoffmann, J. A. Sensing and signaling during infection in *Drosophila*. *Curr. Opin. Immunol.* **17**, 11–17 (2005).
6. Takeda, K. & Akira, S. TLR signaling pathways. *Semin. Immunol.* **16**, 3–9 (2004).
7. Nau, G. J. et al. Human macrophage activation programs induced by bacterial pathogens. *Proc. Natl Acad. Sci. USA* **99**, 1503–1508 (2002).
8. Werner, T. Target gene identification from expression array data by promoter analysis. *Biomol. Eng.* **17**, 87–94 (2001).

9. Mayr, B. & Montminy, M. Transcriptional regulation by the phosphorylation-dependent factor CREB. *Nature Rev. Mol. Cell Biol.* **2**, 599–609 (2001).
10. Yan, C., Lu, D., Hai, T. & Boyd, D. D. Activating transcription factor 3, a stress sensor, activates p53 by blocking its ubiquitination. *EMBO J.* **24**, 2425–2435 (2005).
11. Ishiguro, T. *et al.* Identification of genes differentially expressed in B16 murine melanoma sublines with different metastatic potentials. *Cancer Res.* **56**, 875–879 (1996).
12. Ishiguro, T., Nagawa, H., Naito, M. & Tsuruo, T. Inhibitory effect of ATF3 antisense oligonucleotide on ectopic growth of HT29 human colon cancer cells. *Jpn. J. Cancer Res.* **91**, 833–836 (2000).
13. Kawauchi, J. *et al.* Transcriptional repressor activating transcription factor 3 protects human umbilical vein endothelial cells from tumor necrosis factor- $\alpha$ -induced apoptosis through down-regulation of p53 transcription. *J. Biol. Chem.* **277**, 39025–39034 (2002).
14. Hartman, M. G. *et al.* Role for activating transcription factor 3 in stress-induced beta-cell apoptosis. *Mol. Cell Biol.* **24**, 5721–5732 (2004).
15. Shannon, P. *et al.* Cytoscape: a software environment for integrated models of biomolecular interaction networks. *Genome Res.* **13**, 2498–2504 (2003).
16. Thorsson, V. T., Hörnquist, M., Siegel, A. F. & Hood, L. Reverse engineering galactose regulation in yeast through model selection. *Stat. Appl. Gen. Mol. Biol.* **4**, 1–24 (2005).
17. Bonneau, R. *et al.* The Inferelator: an algorithm for learning parsimonious regulatory networks from systems-biology data-sets *de novo*. *Genome Biol.* **7**, R36–R42 (2006).
18. Hua, B. *et al.* A splice variant of stress response gene ATF3 counteracts NF- $\kappa$ B-dependent anti-apoptosis through inhibiting recruitment of CREB-binding protein/p300 coactivator. *J. Biol. Chem.* **281**, 1620–1629 (2006).
19. Furumatsu, T. *et al.* Sox9 and p300 cooperatively regulate chromatin-mediated transcription. *J. Biol. Chem.* **280**, 35203–35208 (2005).
20. Gilchrist, M., McCauley, S. D. & Befus, A. D. Expression, localization, and regulation of NOS in human mast cell lines: effects on leukotriene production. *Blood* **104**, 462–469 (2004).
21. Thijs, G. *et al.* INCLUSive: INtegrated Clustering, Upstream sequence retrieval and motif Sampling. *Bioinformatics* **18**, 331–332 (2002).
22. Frith, M. C. *et al.* Detection of functional DNA motifs via statistical over-representation. *Nucleic Acids Res.* **32**, 1372–1381 (2004).
23. Matys, V. *et al.* TRANSFAC: transcriptional regulation, from patterns to profiles. *Nucleic Acids Res.* **31**, 374–378 (2003).
24. Lewis, S. E. *et al.* Apollo: a sequence annotation editor. *Genome Biol.* **3**, research0082 (2002).
25. Yang, E. *et al.* Decay rates of human mRNAs: correlation with functional characteristics and sequence attributes. *Genome Res.* **13**, 1863–1872 (2003).
26. Cawley, S. *et al.* Unbiased mapping of transcription factor binding sites along human chromosomes 21 and 22 points to widespread regulation of noncoding RNAs. *Cell* **116**, 499–509 (2004).
27. Kim, T. H. *et al.* A high-resolution map of active promoters in the human genome. *Nature* **436**, 876–880 (2005).

**Supplementary Information** is linked to the online version of the paper at [www.nature.com/nature](http://www.nature.com/nature).

**Acknowledgements** We acknowledge A. Ozinsky, I. Shmulevich, W. Longabaugh and L. Hood for discussions. We thank A. Nachman, A. Clark and C. Baldwin for technical assistance. This work was supported by a Fellowship from the Alberta Heritage Foundation for Medical Research (to M.G.) and the NIH (to A.A.)

**Author Information** Reprints and permissions information is available at [npg.nature.com/reprintsandpermissions](http://npg.nature.com/reprintsandpermissions). The authors declare no competing financial interests. Correspondence and requests for materials should be addressed to A.A. ([aaderem@systemsbiology.org](mailto:aaderem@systemsbiology.org)).

## CORRIGENDUM

doi:10.1038/nature06807

**Depth of a strong jovian jet from a planetary-scale disturbance driven by storms**

A. Sánchez-Lavega, G. S. Orton, R. Hueso, E. García-Melendo, S. Pérez-Hoyos, A. Simon-Miller, J. F. Rojas, J. M. Gómez, P. Yanamandra-Fisher, L. Fletcher, J. Joels, J. Kemerer, J. Hora, E. Karkoschka, I. de Pater, M. H. Wong, P. S. Marcus, N. Pinilla-Alonso, F. Carvalho, C. Go, D. Parker, M. Salway, M. Valimberti, A. Wesley & Z. Pujic

*Nature* 451, 437–440 (2008)

In Fig. 3a, the descriptions of the continuous and dotted curves were inadvertently swapped. The continuous line corresponds to the modified synthetic thermal profile (storms reaching the 60 mbar level). The dotted line corresponds to the Cassini CIRS thermal profile (storms reaching the 160 mbar level).

## ERRATUM

doi:10.1038/nature06729

**Roquin represses autoimmunity by limiting inducible T-cell co-stimulator messenger RNA**

Di Yu, Andy Hee-Meng Tan, Xin Hu, Vicki Athanasopoulos, Nicholas Simpson, Diego G. Silva, Andreas Hutloff, Keith M. Giles, Peter J. Leedman, Kong Peng Lam, Christopher C. Goodnow & Carola G. Vinuesa

*Nature* 450, 299–303 (2007)

In this Letter, some axis labels in Figs 3 and 4 were inadvertently mislabelled. In Fig 3d, the labels on the *x* axes of the three graphs should read 'Hi Low Nil' instead of 'Hi Low Ni'. The *x* axes of the bar graphs in Fig. 4a (right and left panels) and Fig. 4b (right panel) should read 'Hi Low Nil' instead of 'Hi Low Hi'.

## CORRIGENDUM

doi:10.1038/nature06728

**The nonlinear Fano effect**

M. Kroner, A. O. Govorov, S. Remi, B. Biedermann, S. Seidl, A. Badolato, P. M. Petroff, W. Zhang, R. Barbour, B. D. Gerardot, R. J. Warburton & K. Karrai

*Nature* 451, 311–314 (2008)

The experiment measures the differential laser transmission through the quantum dot between the on- and off-exciton resonance condition. As a result, the origin in Fig. 2a–h corresponds to the zero of the measured differential transmission and does not exclude the existence of constant background absorption. It is therefore important to note that the undershoot in the Fano spectra does not correspond to a negative absorption (that is, an optical gain), but is consistent with the continuum broadband background absorption, as analysed in our observation of the nonlinear Fano effect. Similarly, the theoretical graphs in Fig. 2i–n are also given for the differential transmission.

## CORRIGENDUM

doi:10.1038/nature06779

**Systems biology approaches identify ATF3 as a negative regulator of Toll-like receptor 4**

Mark Gilchrist, Vesteynn Thorsson, Bin Li, Alistair G. Rust, Martin Korb, Jared C. Roach<sup>1</sup>, Kathleen Kennedy, Tsonwin Hai, Hamid Bolouri & Alan Aderem

<sup>1</sup>Institute for Systems Biology, Seattle, Washington 98103, USA.*Nature* 441, 173–178 (2006)

In this Article, Jared C. Roach was inadvertently omitted from the list of authors. He was responsible for designing the immune-specific array for ChIP-to-chip analysis. J.C.R. received support from the National Institute of Allergy and Infectious Diseases, National Institutes of Health.